

UKAEA-CCFE-PR(21)02

Shuo Wang, Yueqiang Liu, Guoliang Xia, X. M. Song,
G. Z. Hao, L. Li, B. Li, N. Zhang, G. Q. Dong, X. Bai, G.
Y. Zheng

Modeling active control of resistive wall mode with power saturation and sensor noise on HL-2M

Enquiries about copyright and reproduction should in the first instance be addressed to the UKAEA Publications Officer, Culham Science Centre, Building K1/O/83 Abingdon, Oxfordshire, OX14 3DB, UK. The United Kingdom Atomic Energy Authority is the copyright holder.

The contents of this document and all other UKAEA Preprints, Reports and Conference Papers are available to view online free at scientific-publications.ukaea.uk/

Modeling active control of resistive wall mode with power saturation and sensor noise on HL-2M

Shuo Wang, Yueqiang Liu, Guoliang Xia, X. M. Song, G. Z. Hao, L. Li, B. Li, N. Zhang, G. Q. Dong, X. Bai, G. Y. Zheng

Modeling active control of resistive wall mode with power saturation and sensor noise on HL-2M

S. Wang¹, Y.Q. Liu², G.L. Xia³, X.M. Song¹, G.Z. Hao¹, L. Li⁴,
B. Li¹, N. Zhang¹, G.Q. Dong¹, X. Bai¹ and G.Y. Zheng¹

¹Southwestern Institute of Physics, P. O. Box 432, Chengdu 610041, China

²General Atomics, PO Box 85608, San Diego, CA 92186-5608, USA

³CCFE, Culham Science Centre, Abingdon, OX14 3DB, UK

⁴Donghua University, College of Science, Shanghai 201620, China

E-mail: wangsw@swip.ac.cn, liuy@fusion.gat.com

November 2020

Abstract. The resistive wall mode (RWM) control on the HL-2M tokamak is simulated with the MARS-F code [Liu Y Q *et al* 2000 *Phys. Plasmas* **7** 3681], aiming at quantifying control current and voltage requirements when more realistic issues are taken into account, i.e. the control power saturation and the sensor signal noise. The fluid model predicts a narrow stability region for the $n = 1$ RWM without magnetic feedback, in the 2D parameter space of the plasma pressure versus the toroidal flow speed. Magnetic feedback can fully stabilize the RWM on HL-2M. Without considering the voltage limitation and the sensor signal noise, we find that plasma flow helps active control of the mode, by reducing the required critical feedback gain for both flux-to-current and flux-to-voltage control schemes. In the absence of the sensor signal noise, the lowest control voltage saturation level, below which the RWM control is lost, is found to roughly satisfy a linear relation to the plasma flow frequency, indicating that subsonic plasma flow is effective in relaxing the control power requirement for the RWM feedback stabilization. The presence of the sensor signal noise substantially modifies the feedback results. A statistical study finds that the sensor signal noise, with the standard deviation of 0.1 G on HL-2M, roughly doubles the required control voltage for successful mode control. The synergistic stabilization effect due to plasma flow is somewhat weakened by the presence of the sensor signal noise. At a given rotation, the tolerable voltage limit generally increases with increasing feedback gain due to the sensor signal noise.

1. Introduction

The resistive wall mode (RWM) is one of the major instabilities of concern in advanced tokamak (AT) scenarios, which aim at steady state and high performance operations. The requirement for steady state implies fully non-inductive current drive including maximizing the bootstrap current fraction, which in turn requires high plasma pressure [1]. For this reason, the AT scenarios are often designed to have the plasma pressure exceeding the Troyon no wall limit [2], resulting in unstable ideal external kink and

1
2
3 *Modeling active control of resistive wall mode with power saturation and sensor noise on HL-2M2*

4 resistive wall mode. An unstable RWM may cause major disruption of the tokamak
5 plasma discharge, since it cannot easily non-linearly saturate by itself. Extensive
6 experimental and theoretical studies have shown that the RWM can be stabilized by
7 plasma flow in conjunction with various passive free energy dissipation mechanisms
8 [3–13] and/or magnetic feedback [14–26].
9

10 This work specifically focuses on numerical investigation of the RWM stability on
11 the HL-2M tokamak. HL-2M is a medium-sized copper-conductor tokamak [27,28], with
12 the design (maximal) plasma current of $I_p = 2.5$ (3) MA, toroidal field $B_0 = 2.2$ (3) T,
13 major radius $R_0 = 1.78$ m, minor radius $a = 0.65$ m, and elongation $\kappa = 1.8$. In HL-
14 2M, the up-down symmetric poloidal field coil system is located between the toroidal
15 field coils and the vacuum vessel, allowing flexibility of operating in various divertor
16 configurations including the snowflake configurations [29]. One of the key objectives
17 of the HL-2M design is to study high beta, high performance fusion plasmas. The
18 first plasma has recently been successfully produced on this device. Controlling the
19 RWM instability is one of the main research topics in HL-2M during the later phase of
20 operation. This motivates our present modeling work, where we consider both passive
21 and active control of the RWM for a reference, high-beta target plasma designed on
22 HL-2M.
23
24
25
26
27
28

29 Previous studies have shown that combination of passive stabilization and active
30 control provides an effective way to suppress the RWM [30–32]. In particular, Ref. [32]
31 investigated the combined effects of toroidal plasma flow, drift kinetic effects from
32 thermal particles, and magnetic feedback on the RWM stability in an HL-2M plasma.
33 This work extends the study of Ref. [32], by considering additional physics elements,
34 mostly on the control side, that were neglected in the previous work. As we shall
35 show, inclusion of these extra elements results in new physics effects on the RWM
36 stability. More importantly, the present study presents an important step towards
37 realistic modeling of the RWM control on HL-2M. The new physics effects considered
38 in this work include
39
40
41

- 42 • Effect of power saturation on the active control system, where we investigate what
43 happens to the RWM feedback, if the power supply limit is reached in future
44 experiments
45
- 46 • Effect of sensor signal noise on the control system, where we focus on the high-
47 frequency white noise with Gaussian characteristics
48
- 49 • Quantitative comparison of the active control performance between the so-called
50 flux-to-voltage and flux-to-current control schemes
51
- 52 • Initial value simulation of the close-loop system with or without assuming toroidal
53 equilibrium flow of the plasma, allowing quantification of the control voltage and
54 current requirements for the RWM feedback on HL-2M. This is different from the
55 eigenvalue approach taken in the previous work [32].
56
57

58 We note that similar initial value simulations for the RWM control have previously
59 been carried out for a JET-like plasma [25] and for the ITER 9 MA advanced scenario
60

1
2
3 *Modeling active control of resistive wall mode with power saturation and sensor noise on HL-2M3*

4 [26], but assuming vanishing plasma equilibrium flow. This work presents the first
5 numerical study of the synergistic effect by both magnetic feedback and plasma flow on
6 the RWM stability, in the presence of control power saturation and sensor signal noise.
7 As for the modeling tool, we utilize the MARS-F code [15] updated to accommodate
8 initial value simulations for close-loop control systems.
9

10
11 The remainder of the paper is organized as follows. Section 2 briefly introduces
12 the magneto-hydrodynamic (MHD) and control models in MARS-F. Section 3 reports
13 numerical results on passive and active control, as well as the combination of both, on
14 the RWM stability on HL-2M. We draw conclusion in Sec. 4.
15
16
17

18 2. Computational model

19
20 The MARS-F code is adopted to compute the growth rate of the RWM and to solve the
21 feedback equation. In this work, we describe the RWM by an ideal MHD model
22

$$23 \quad (\tilde{\gamma} + in\Omega)\xi = \mathbf{v} + (\xi \cdot \nabla\Omega)R^2\nabla\phi \quad (1)$$

$$24 \quad \rho(\tilde{\gamma} + in\Omega)\mathbf{v} = -\nabla p + \mathbf{j} \times \mathbf{B} + \mathbf{J} \times \mathbf{b} - \rho[2\Omega\hat{\mathbf{Z}} \times \mathbf{v} + (\mathbf{v} \cdot \nabla\Omega)R^2\nabla\phi] - \nabla \cdot \mathbf{\Pi} \quad (2)$$

$$25 \quad (\tilde{\gamma} + in\Omega)\mathbf{b} = \nabla \times (\mathbf{v} \times \mathbf{B}) + (\mathbf{b} \cdot \nabla\Omega)R^2\nabla\phi \quad (3)$$

$$26 \quad (\tilde{\gamma} + in\Omega)p = -(\mathbf{v} \cdot \nabla)P - \Gamma P \nabla \cdot \mathbf{v} \quad (4)$$

$$27 \quad \mu_0\mathbf{j} = \nabla \times \mathbf{b} \quad (5)$$

28
29 where $\tilde{\gamma} = \gamma + i\omega_r$ is the eigenvalue of the mode, to be corrected by a Doppler
30 shift frequency $in\Omega$ associated with toroidal flow of the plasma. Here, n is the
31 toroidal mode number and Ω the plasma rotation frequency along the toroidal angle ϕ .
32 Quantities in lower case, $(\xi, \mathbf{v}, \mathbf{j}, \mathbf{b}, p)$, denote the plasma displacement, the perturbed
33 velocity, current, magnetic field and plasma pressure, respectively. The upper case
34 quantities $(\mathbf{B}, \mathbf{J}, P)$ denote the plasma equilibrium magnetic field, current, and pressure,
35 respectively. Other quantities include the plasma equilibrium mass density ρ , the plasma
36 major radius R , the unit vector in the vertical direction $\hat{\mathbf{Z}}$.
37

38 The viscous stress tensor $\mathbf{\Pi}$ represents the ion-Landau damping physics on the
39 RWM [4], with $\nabla \cdot \mathbf{\Pi} = \kappa_{//}\sqrt{\pi}|k_{//}v_{th}^i|\rho\mathbf{v}_{//}\hat{\mathbf{b}}\hat{\mathbf{b}}$. Here, $\kappa_{//}$ is a numerical coefficient
40 specifying the damping strength. $k_{//}$ is the parallel wave number, v_{th}^i the ion thermal
41 velocity, $\mathbf{v}_{//}$ the perturbed parallel velocity of the plasma, and $\hat{\mathbf{b}} = \mathbf{B}/B$.
42

43 The MARS-F code directly solves the above perturbed MHD equations in the
44 plasma region, together with the following feedback equation in the vacuum region
45 outside the plasma
46

$$47 \quad \frac{d\Psi_f}{dt} + R_f I_f = V_f = -G b_s \quad (6)$$

48 where Ψ_f is the perturbed magnetic flux through the active coils. I_f, R_f, V_f are the
49 current, resistance and voltage of the active coils, respectively. G is the feedback gain
50 which generally takes complex values. In the MARS-F formulation and throughout this
51
52
53
54
55
56
57
58
59
60

Modeling active control of resistive wall mode with power saturation and sensor noise on HL-2M4

paper, G is normalized by R_0^2/τ_A , rendering the feedback gain a dimensionless quantity. b_s is the sensor signal, defined as the point-wise poloidal magnetic field perturbation in this work.

The above control logic, referred to as the flux-to-voltage control, applies to linear close-loop systems. In more general cases, where the control voltage V_f is constrained by the power limitation V_f^{lim} , we assume

$$V_f = \begin{cases} V_f^{\text{lim}}, & \text{if } V_f \geq V_f^{\text{lim}} \\ -V_f^{\text{lim}}, & \text{if } V_f \leq -V_f^{\text{lim}} \\ -Gb_s, & \text{if } |V_f| < V_f^{\text{lim}}. \end{cases} \quad (7)$$

Furthermore, in the presence of the sensor signal noise, we assume $b_s = b_s^0 + b_s^{\text{noise}}$, where the noise contribution b_s^{noise} satisfies Gaussian distribution $N(0, \sigma^2)$ with zero mean and standard deviation of σ . The latter is a parameter that we shall scan in our initial value simulations.

Before showing numerical results, we remark that Eq. (6) is effectively converted into the flux-to-current control logic by neglecting the first term in the left hand side. This is what we shall employ when compare the two control schemes later on.

3. Numerical results

In what follows, we consider an AT plasma scenario designed for HL-2M, with the target plasma reaching the normalized beta value of $\beta_N \equiv \beta(\%)a(\text{m})B_0(\text{T})/I_p(\text{MA}) = 4.31$. Here, β is the plasma pressure normalized by the toroidal magnetic pressure, $a = 0.59$ m the plasma minor radius, $B_0 = 2.2$ T the vacuum toroidal magnetic field at the major radius of 1.78 m, and $I_p = 2$ MA the plasma current. The target equilibrium exceeds the no-wall beta limit of $\beta_N^{\text{NW}} = 3.49$ for the onset of the $n = 1$ ideal external kink instability, but is below the ideal-wall limit of $\beta_N^{\text{IW}} = 5.5$. Defining the pressure scaling factor $C_\beta \equiv (\beta_N - \beta_N^{\text{NW}})/(\beta_N^{\text{IW}} - \beta_N^{\text{NW}})$, the target plasma corresponds to $C_\beta \sim 0.4$.

The plasma boundary shape and the wall shape are shown in Fig. 1. Considered here is a double-null plasma configuration. On HL-2M, the vacuum vessel, with a double-shell structure, serves as the main conducting structure. Each vessel shell is made of 5 mm thick Inconel 625 material with resistivity of $1.29 \mu\Omega \cdot \text{m}$ [28].

The RWM feedback system consists of two sets of active coils and one set of sensor coils, both located at the low field side just inside the inner wall. As preliminary designed on HL-2M, the poloidal angle of the center of each set of active coils is $|\theta_c| = 29.9^\circ$ (as measured in geometric poloidal angle θ), with the poloidal coverage of $\Delta\theta = 21.8^\circ$. The sensor coils are located at the outboard mid-plane measuring the perturbation in the poloidal field component. This choice is motivated by the well established result that the internal poloidal sensors perform much superior over the radial sensors for the RWM control [15]. Note that in this study, we assume that the single sensor signal is used to drive the coil currents in both upper and lower rows of active coils via two

Modeling active control of resistive wall mode with power saturation and sensor noise on HL-2M5

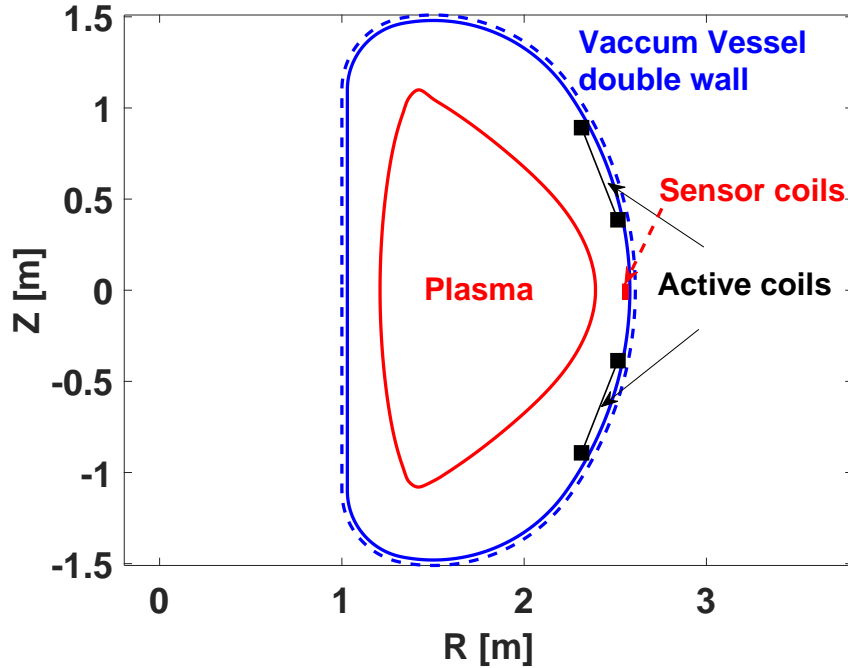


Figure 1. Basic geometry of the RWM control on HL-2M: the plasma boundary shape (red solid line) for a 2 MA double-null equilibrium from the high performance scenario, the shape of the conducting vacuum vessel with double-wall structure (blue solid and dashed lines), the locations of the active (black dots) and sensor (red dot) coils. The poloidal angle of the center of the active coils is $|\theta_c| = 29.9^\circ$, with the poloidal coverage of $\Delta\theta = 21.8^\circ$.

independent feedback gains, resulting in the so-called multi-input-single-output (MISO) control scheme.

The choice of the radial location (i.e. in-vessel) for active coils here follows that in ITER, where magnetic coils are designed to control the edge localized mode (ELM) and the RWM. Compared to a design where the active coils are located outside the vacuum vessel, the in-vessel coils offer better coupling of the control field to the plasma. In particular, the overall time lag of the close-loop system is reduced by avoiding the field penetration through the wall. On the other hand, the obvious disadvantages of the in-vessel coil design, in particular for future fusion reactors, are the space constraint and the irradiation problem. These are not severe issues though for HL-2M.

3.1. RWM stabilization by plasma flow

We start with the open-loop stability problem for the RWM, but taking into account the plasma flow effect. We first consider the target equilibrium with $C_\beta \sim 0.4$. The plasma toroidal rotation profile is numerically assumed as shown in Fig. 2, where the on-axis rotation frequency is normalized to unity. In what follows, we shall scan the on-axis rotation amplitude while fixing the overall radial profile shape. The toroidal

Modeling active control of resistive wall mode with power saturation and sensor noise on HL-2M6

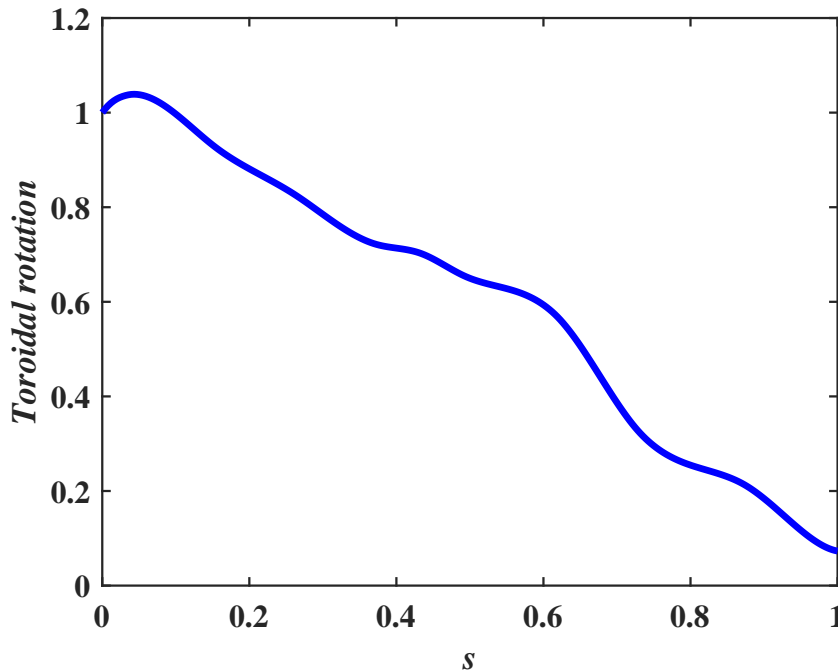


Figure 2. Radial profile of the toroidal rotation frequency chosen for the modeling in HL-2M. The radial coordinate is labeled by $s \equiv \sqrt{\psi_p}$, with ψ_p being the normalized equilibrium poloidal flux. The on-axis ($s = 0$) value of the rotation is normalized to unity here.

flow amplitude is estimated to be in the order of 10^5 rad/s, given the available neutral beam injection power on HL-2M.

Figure 3 reports the MARS-F computed growth rate $\gamma\tau_w$ and real frequency $\omega_r\tau_w$ of the $n = 1$ RWM in the target plasma, while scanning the on-axis rotation frequency Ω_0 . The latter is normalized by the toroidal Alfvén frequency $\Omega_A = v_A/R_0$ with $v_A \equiv B_0/\sqrt{\mu_0\rho_0}$, where μ_0 is the permeability of free space and ρ_0 the mass density at the center of the plasma. A strong parallel sound wave damping model is adopted here, with the damping coefficient $\kappa_{//} = 1.5$. We remark that there is no unique value for $\kappa_{//}$. It has previously been thought that $\kappa_{//} \ll 1$ when the plasma toroidal flow speed is well below the sound speed [33]. On the other hand, there are regions close to resonant surfaces where the parallel phase velocity in the plasma frame is large enough to resonate with thermal particles, and where the local damping is strong [34]. The large value of $\kappa_{//}$ used here mimics strong ion Landau damping. According to the fluid RWM theory, the critical rotation for the mode stabilization depends on this damping coefficient [35].

Figure 3 shows that the critical on-axis rotation for the RWM stabilization is about 6% of the Alfvén frequency on HL-2M, assuming the ideal MHD model. This value is consistent with the findings from Refs. [3] and [4]. We emphasize, however, that the critical rotation is significantly altered by considering the drift kinetic stabilization of

Modeling active control of resistive wall mode with power saturation and sensor noise on HL-2M7

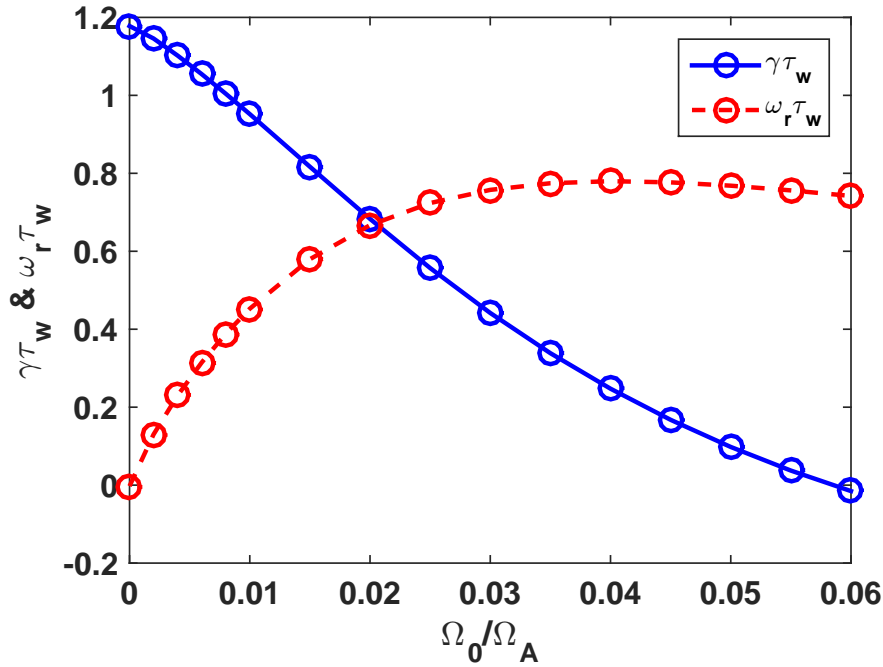


Figure 3. The MARS-F computed open-loop growth rate (solid line) and mode frequency (dashed line) of the $n = 1$ RWM, with varying on-axis toroidal rotation frequency Ω_0 (normalized by the Alfvén frequency Ω_A) while fixing the overall rotation profile as shown in Fig. 2. Considered here is the target equilibrium ($C_\beta = 0.4$) designed on HL-2M. The parallel viscosity coefficient is assumed to be $\kappa_{//} = 1.5$. The double-wall radial locations are assumed as $d/a = 1.30$ and 1.35 .

the RWM due to thermal particles, as has already been demonstrated in Ref. [32] for HL-2M. By neglecting the drift kinetic effects in this study, we obtain more conservative prediction for the RWM instability on HL-2M, as long as the passive stabilization is concerned.

Next, we expand the parametric study reported in Fig. 3, by considering a family of equilibria obtained with the pressure scaling factor C_β . This leads to a 2D parameter scan in the $C_\beta - \Omega_0/\Omega_A$ space, with the computed stability results reported in Fig. 4. The RWM growth rate rapidly increases with C_β as the latter approaches 1 (the ideal-wall beta limit). Passive stabilization alone, by the plasma flow, becomes more difficult at higher plasma pressures. In fact, only a narrow window exists in this 2D parameter space, where the RWM instability is fully suppressed (again according to the fluid theory) on HL-2M. The marginal stability curve, plotted as the white dashed line in Fig. 4(a), is well approximated by a linear relation $\Omega_0/\Omega_A = 0.152 C_\beta$, quantifying the required critical rotation speed for the RWM stabilization on HL-2M, as the plasma pressure is increased. On the other hand, we also note that the sub-sonic toroidal flow is generally effective in reducing the mode growth rate even at high C_β . For instance, at $C_\beta = 0.9$, the normalized mode growth rate $\gamma\tau_w$ is reduced from 11.38 to 1.67, as the on-axis rotation frequency Ω_0/Ω_A increases from 0 to 0.02.

Modeling active control of resistive wall mode with power saturation and sensor noise on HL-2M8

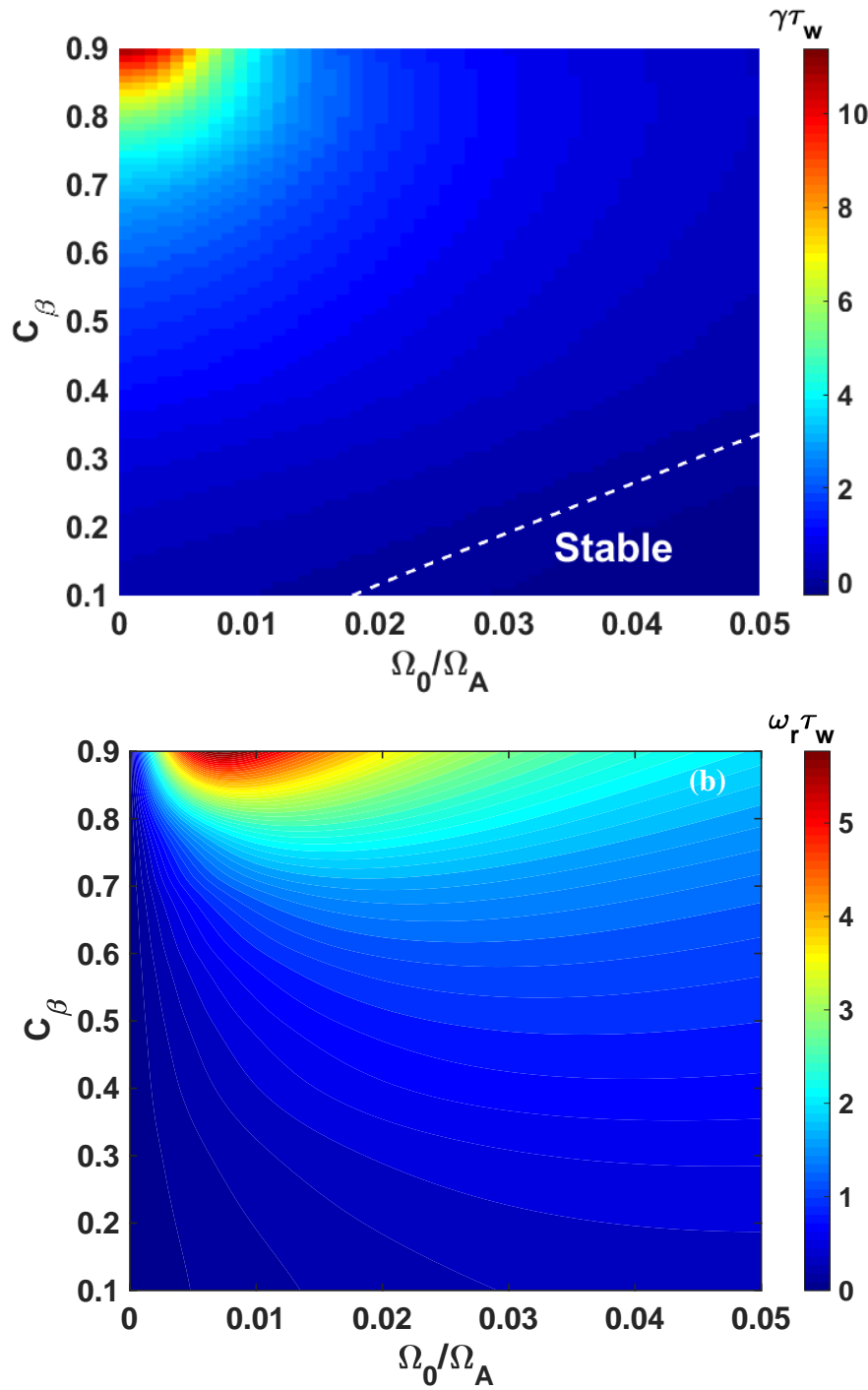


Figure 4. Contour plots of (a) growth rate, and (b) mode frequency, of the MARS-F computed open-loop $n = 1$ RWM, in the 2D parameter space of the on-axis toroidal rotation frequency Ω_0 and the equilibrium pressure scaling factor C_β . The dashed white line in (a) indicates the stability boundary. The other parameters are the same as that in Fig. 3.

Modeling active control of resistive wall mode with power saturation and sensor noise on HL-2M9

Figure 4(b) shows that the mode frequency is almost the same order as the RWM growth rate, and generally scales with C_β . For relatively low C_β equilibria, the mode frequency monotonically increases with the plasma rotation speed, while it becomes non-monotonic in cases with higher C_β values.

3.2. RWM stabilization by feedback control: eigenvalue approach

Now we investigate the possibility of feedback stabilization of the $n = 1$ RWM on HL-2M, following the eigenvalue approach first which can only be employed to study linear control problem. Different from the previous work [32], we shall consider and compare two control schemes, i.e. the flux-to-voltage versus the flux-to-current control. The latter is what was assumed in Ref. [32].

With a MISO control system, it is important to choose the phase of the (complex) feedback gains associated with the upper and lower rows of the active coils. As shown in Fig. 5, at a given gain amplitude ($|G| = 0.3$) for both rows of active coils, the close-loop growth rate is sensitive to the choice of the gain phase. Feedback has almost no effect on the mode stabilization (compared to the open-loop value as reported in Fig. 3), if the gain phase is not properly chosen. The optimal gain phase is $\phi_U = -\phi_L = 120^\circ$ for the case shown in Fig. 5, where we have assumed the flux-to-voltage control scheme. Interestingly, the same optimal gain phase was found with the flux-to-current control scheme [32]. We also mention that the optimal gain phase is generally not sensitive to the gain amplitude $|G|$ but can be altered by the toroidal plasma flow. A vanishing equilibrium flow is assumed in Fig. 5.

Next, fixing the feedback gain phase to the optimal value as found from Fig. 5, we investigate the RWM stabilization with increasing gain amplitude. Figure 6 compares the feedback performance between the two control schemes as mentioned before. The open-loop growth rate (at $|G| = 0$) of the RWM is lower in the flux-to-voltage control scheme as compared to the flux-to-current control. This is because in the former, the active coils act as additional passive conductors (on top of the resistive wall), reducing the mode growth rate. A systematic study of this additional passive stabilization mechanism, where the relative conductivities between the active coils and the resistive wall were scanned, was reported in Ref. [26].

We note that the close-loop growth rates converge to the same value between the two control schemes, as we increase the feedback gain amplitude as shown in Fig. 6. This can be analytically understood. Indeed, Eq. (6) shows that the critical feedback gain should be the same between the two control schemes, since the first term from the left hand side of the equation disappears at the marginal stability point. This means that both control schemes yield the same critical gain value for the mode stabilization, as confirmed by Fig. 6. We emphasize that the above statement is valid only if the mode has vanishing real frequency at marginal stability point. Finite plasma flow induces finite mode frequency at the marginal stability point, and consequently will lead to different critical gain amplitude for the mode stabilization between the two control schemes. This

Modeling active control of resistive wall mode with power saturation and sensor noise on HL-2M10

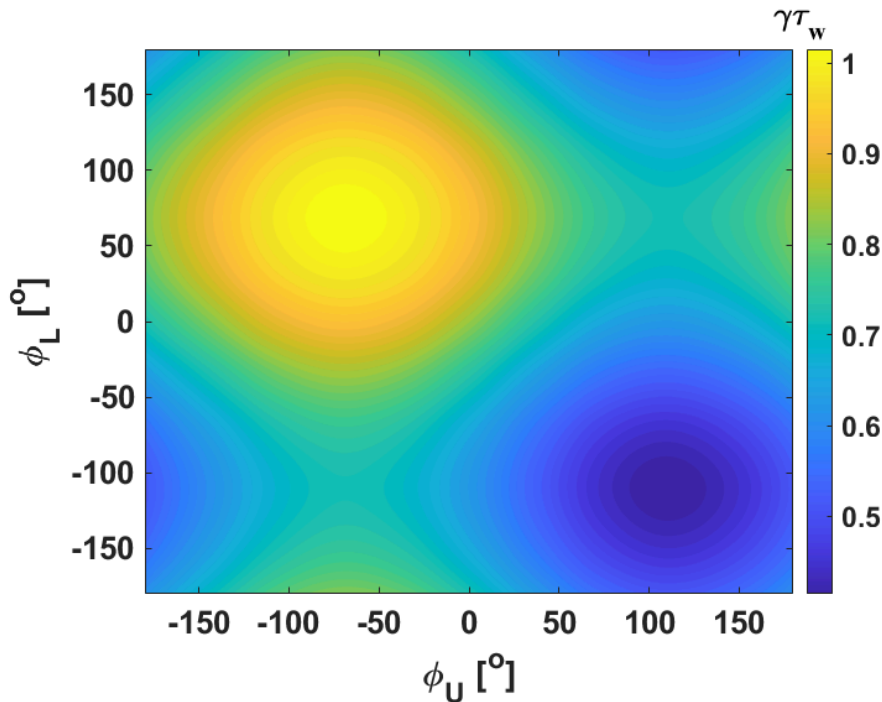


Figure 5. Contour plots of the growth rate of the close-loop $n = 1$ RWM, in the 2D parameter space of the feedback gain phase (ϕ_U, ϕ_L) for the upper and lower rows of active coils, respectively. Considered is the flux-to-voltage control scheme with the proportional gain amplitude fixed at $|G| = 0.3$. Assumed is vanishing equilibrium flow. Other parameters are the same as that in Fig. 3.

will be demonstrated in the following sub-section.

3.3. Synergistic stabilization of RWM by feedback and plasma flow

We now compare feedback stabilization of the RWM for the target HL-2M plasma, between the flux-to-voltage and flux-to-current control schemes in the presence of the plasma flow. We will follow both eigenvalue and initial value approaches in this sub-section.

Figure 7 compares the MARS-F computed close-loop growth rate between the two control schemes, while scanning the feedback gain amplitude assuming different toroidal rotation frequencies. The gain phase is fixed at the optimal values obtained assuming vanishing flow (Fig. 5). Despite the fact that the optimal gain phase is modified by the plasma flow [32], it is reasonable to fix the gain phase during feedback control in practice, even if the plasma rotation is evolving. Figure 7 shows that the RWM on HL-2M is fully stabilized when the feedback gain amplitude exceeds a critical value, $|G_{\text{cri}}|$, with either control scheme. The critical gain value decreases with increasing plasma flow speed. On the other hand, at the same flow speed, the flux-to-voltage control scheme (Fig. 7 (b)) requires less critical gain than the flux-to-current scheme (Fig. 7 (a)), in order to stabilize the RWM.

Modeling active control of resistive wall mode with power saturation and sensor noise on HL-2M11

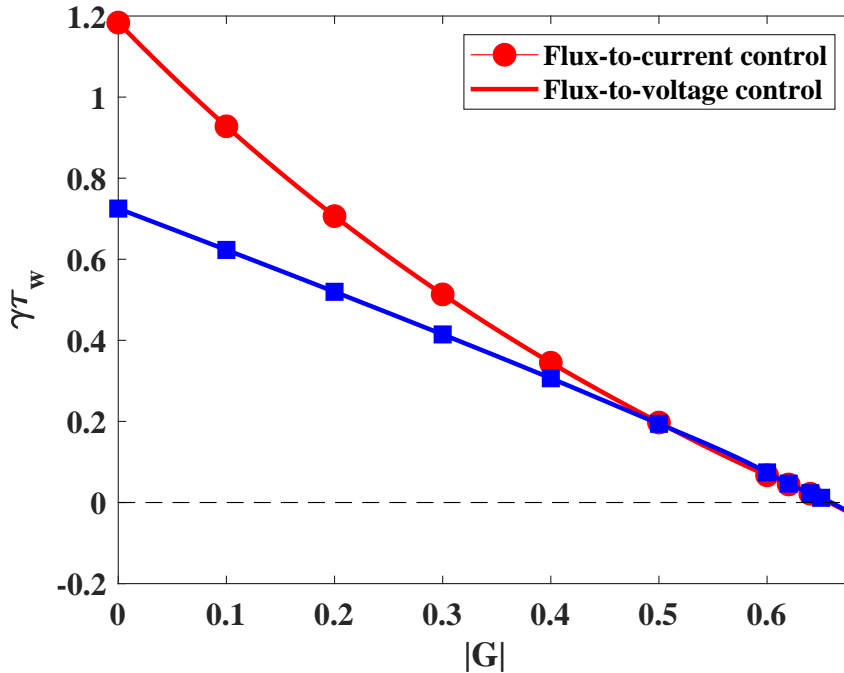


Figure 6. The MARS-F computed close-loop growth rate of the $n = 1$ RWM with increasing feedback gain amplitude $|G|$, for the target equilibrium ($C_\beta = 0.4$) designed on HL-2M. The phase of the feedback gains are fixed at $\phi_U = -\phi_L = 120^\circ$ for the upper and lower rows of active coils, respectively.

The critical gain amplitude can be quantified for the target HL-2M plasma, as a function of the toroidal rotation frequency, by analytically fitting the numerical data shown in Fig. 7. We obtain $|G_{\text{cri}}| = -38.6 (\Omega_0/\Omega_A)^2 - 9.6 \Omega_0/\Omega_A + 0.66$ for the flux-to-current control scheme and $|G_{\text{cri}}| = -47.9 (\Omega_0/\Omega_A)^2 - 11.5 \Omega_0/\Omega_A + 0.66$ for the flux-to-voltage control. Note that these analytic fitting formulae recover the critical gain value at the limit of vanishing flow as reported in Fig. 6, as well as the critical rotation speed without feedback ($|G_{\text{cri}}| = 0$) as shown in Fig. 3.

The eigenvalue approach reported above is good at obtaining the close-loop growth rate and the critical gain values for the mode stabilization, but does not reveal many quantities of practical importance for the RWM control, e.g. the required maximal control voltage and control current, the settling time for a stable control loop after the feedback is switched on, and more generally the overall dynamic behavior of the close-loop system. Initial value simulations are needed for these purposes, even for linear control. We note that some of the control loop characteristics, e.g. the maximal voltage and current requirements, can be recovered based on the eigenvalue approach, by performing inverse Laplace transform of the plasma response transfer function obtained with the eigenvalue approach [36]. This, however, requires the knowledge of open-loop transfer function, which can in principle be obtained with the Padé approximation of the numerically computed eigenvalue data [37]. Nevertheless, initial value simulations,

Modeling active control of resistive wall mode with power saturation and sensor noise on HL-2M12

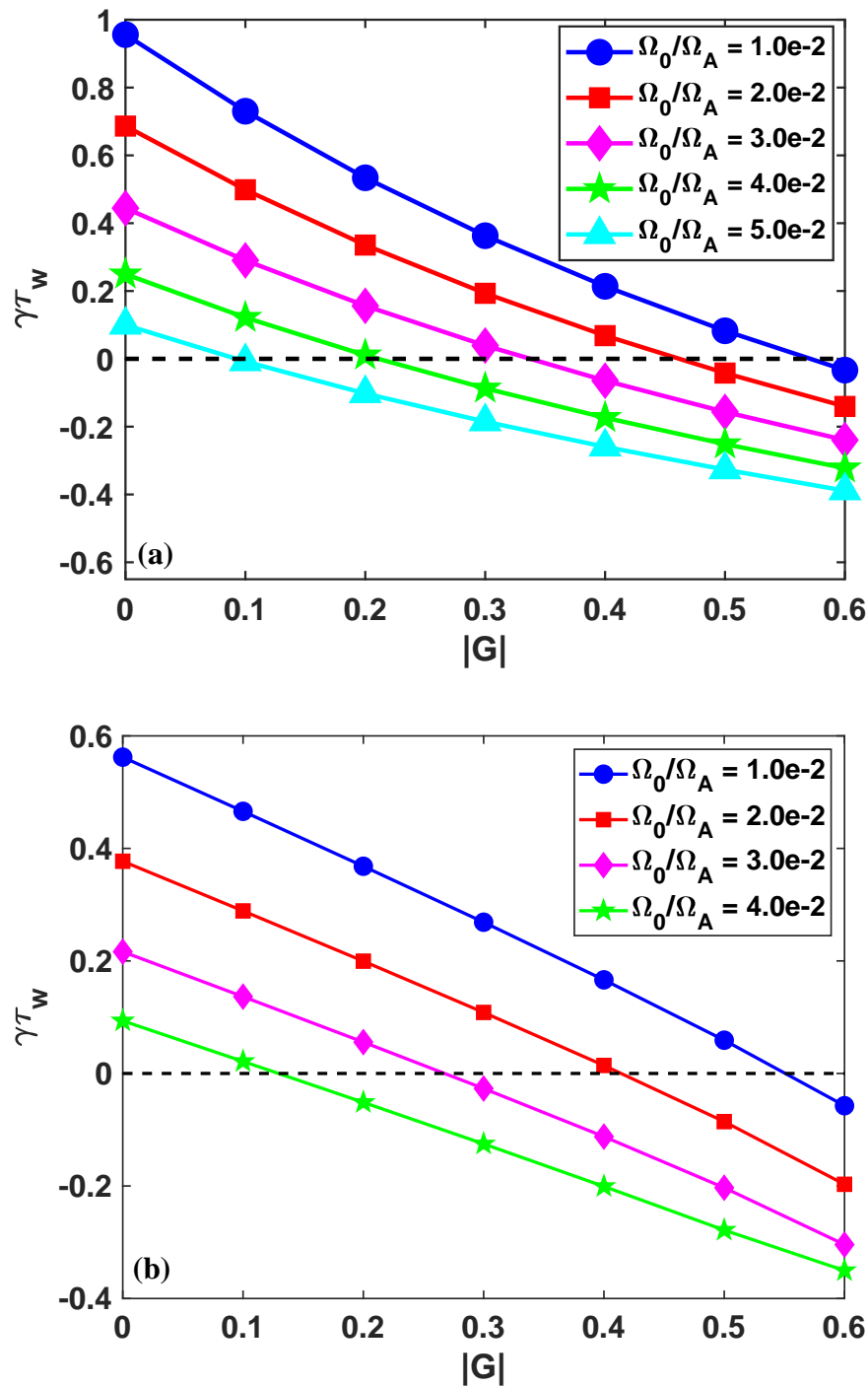


Figure 7. The MARS-F computed close-loop growth rate of the $n = 1$ RWM with increasing proportional gain amplitude, assuming (a) the flux-to-current control scheme and (b) the flux-to-voltage control scheme. Plotted are the different choices of the plasma toroidal rotation frequency. Other parameters are the same as that in Fig. 6.

Modeling active control of resistive wall mode with power saturation and sensor noise on HL-2M13

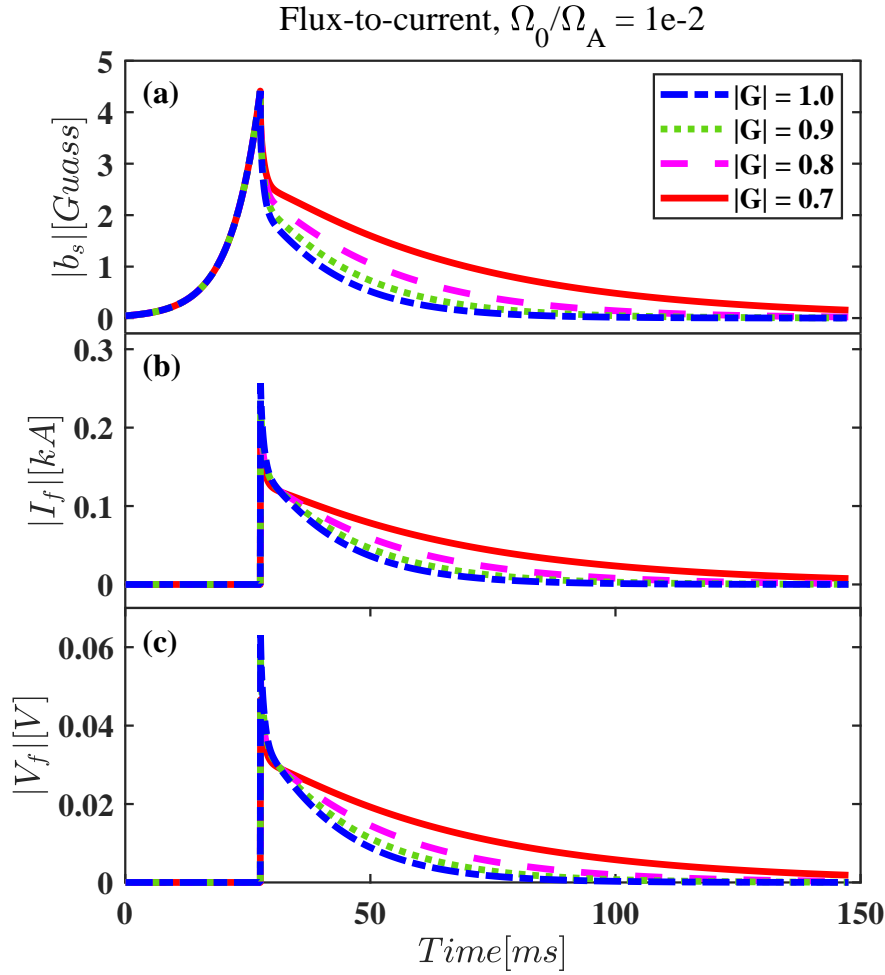


Figure 8. Simulated time traces of the $n = 1$ RWM feedback stabilization by the flux-to-current control scheme, in combination with the plasma toroidal flow. Plotted are the time traces of (a) the amplitude of the poloidal sensor signal, (b) the current amplitude in the active coils, and (c) the voltage of the active coil power supply. The control loop is closed at 25 ms. Different choices of feedback gain amplitude are plotted with different curve styles. The on-axis rotation frequency of $\Omega_0/\Omega_A = 0.01$. Other parameters are the same as that in Fig. 6.

though more time-consuming, offer direct information on the whole dynamics of the feedback system and is of more practical relevance too. In what follows, we focus on initial value simulations of the feedback system for the RWM control on HL-2M.

The simulation results of linear control, without assuming control voltage limitation and sensor signal noise, are reported in Figs. 8 and 9, for the flux-to-current and flux-to-voltage control schemes, respectively. Note that it is the first time we report the initial value simulations with the flux-to-current scheme for the RWM control. With both control schemes, we vary the feedback gain $|G|$ from 0.7 to 1 while fixing the plasma flow speed at $\Omega_0/\Omega_A = 0.01$. These $|G|$ values are larger than the critical gain $|G_{\text{cri}}|$, ensuring close-loop stability.

Modeling active control of resistive wall mode with power saturation and sensor noise on HL-2M14

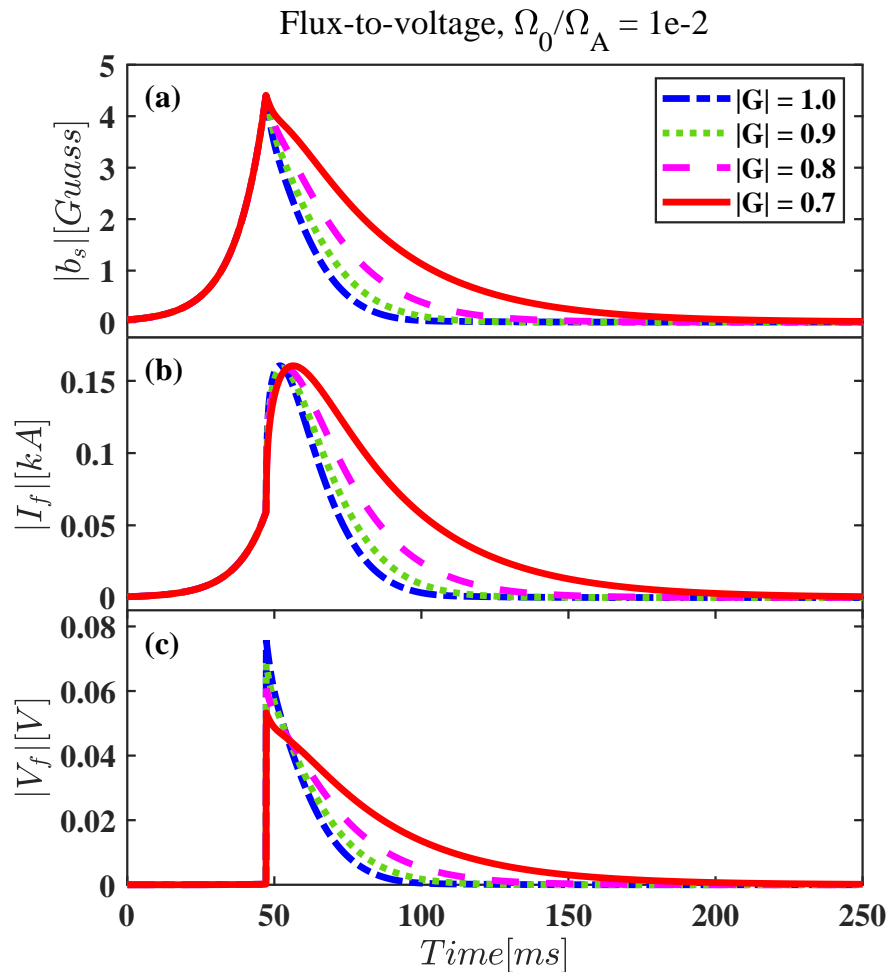


Figure 9. Simulated time traces of the $n = 1$ RWM feedback stabilization by the flux-to-voltage control scheme with the plasma toroidal flow effects. Plotted are the time traces of (a) the amplitude of the poloidal sensor signal, (b) the current amplitude in the active coils, and (c) the voltage of the active coil power supply. The control loop is closed at 48 ms. Different lines show the performances with different choices of feedback gain amplitude. Other parameters are the same as that in Fig. 8.

We first follow the open-loop stage for 25 ms with the flux-to-current control (Fig. 8) and 48 ms with the flux-to-voltage control scheme (Fig. 9), starting from the same initial perturbation amplitude as measured by the sensors (plots (a)). These open-loop time intervals allow the mode to exponentially grow to the same amplitude (~ 4.5 G) between the two schemes, when the control loop is closed. With the chosen gain values, the closed loops indeed become stable, with decreasing settling time at increasing feedback gain. Note that the dynamics of active coil current $I_f(t)$ (plots (b)) are qualitatively different between the two control schemes. At the time when the feedback is switched on, $I_f(t)$ continuously evolves with the flux-to-voltage control scheme. This is because with the latter scheme, control currents are already passively induced in the active coils in the open-loop stage.

Modeling active control of resistive wall mode with power saturation and sensor noise on HL-2M15

Sharp decay of all control signals are found in Fig. 8 with the flux-to-current scheme, right after feedback is switched on. Both the maximal achievable control coil current and voltage are proportional to feedback gain with this scheme. This is not the case with the flux-to-voltage scheme. With the latter, the maximal control voltage increases with feedback gain as well, but the control coil current peaking value always stays the same (the peaking time varies though). For identical feedback gain, the maximal achievable voltage with the flux-to-voltage control is larger than that with the flux-to-current control.

With the flux-to-current control, both control current and voltage experience sudden jumps when the feedback is switched on. This has a significant implication for this control scheme. As has been analytically shown in Ref. [24], an upper limit cannot be imposed to the control current for the flux-to-current control scheme to ensure the close-loop stability. In other words, the control will be lost if the control current saturation is reached for this control scheme. Therefore, in the non-linear control to be studied below, we shall only consider the flux-to-voltage control scheme.

3.4. RWM control with power saturation and sensor noise

First, we perform initial value simulations assuming the control power limitation V_f^{lim} for the active coils, but in the absence of the sensor signal noise. Three examples are compared in Fig. 10. The solid curves indicate the linear control, where no voltage limit is imposed. In this case, the close-loop system achieves a maximal value of voltage, denoted as V_f^{max} , as soon as feedback is switched on. V_f^{max} varies with feedback gain $|G|$ as shown in Fig. 9. Here, we have $V_f^{\text{max}} = 0.07$ V at $|G| = 0.9$. It is evident that the feedback system will lose control when V_f^{lim} is below a critical value V_f^{min} ($=0.054$ in this case). This critical case is shown by dotted curves in Fig. 10, where the control coil voltage saturates all the time and the close-loop RWM rapidly grows, i.e. the mode control is lost. For cases where V_f^{lim} is between V_f^{min} and V_f^{max} , the RWM is eventually feedback stabilized despite the occurrence of temporary voltage saturation during the close-loop simulation. One such example is shown by dashed curves in Fig. 10. Finally, if the control voltage limit is larger than V_f^{max} , the feedback system performs the same way as that without power saturation.

Shown in Fig. 10 are cases with vanishing plasma flow. We have also carried out similar simulations with finite plasma flow for the target HL-2M plasma. The key result of interest, i.e. the V_f^{min} value, is summarized in Fig. 11 versus the on-axis toroidal rotation frequency of the plasma. It is evident that the minimal control voltage needed to stabilize the RWM decreases with increasing plasma rotation. In other words, plasma flow helps to make the close-loop system more tolerable to the control power limitation. It is interesting that the minimal voltage requirement can be well represented by a linear fitting curve (dashed line in Fig. 10) $V_f^{\text{min}} = -1.08 \Omega_0/\Omega_A + 0.054$ for HL-2M. The fact that the proportionality coefficient here is an order one term indicates that the reduction of the minimal voltage is significant even with subsonic plasma flow.

Modeling active control of resistive wall mode with power saturation and sensor noise on HL-2M16

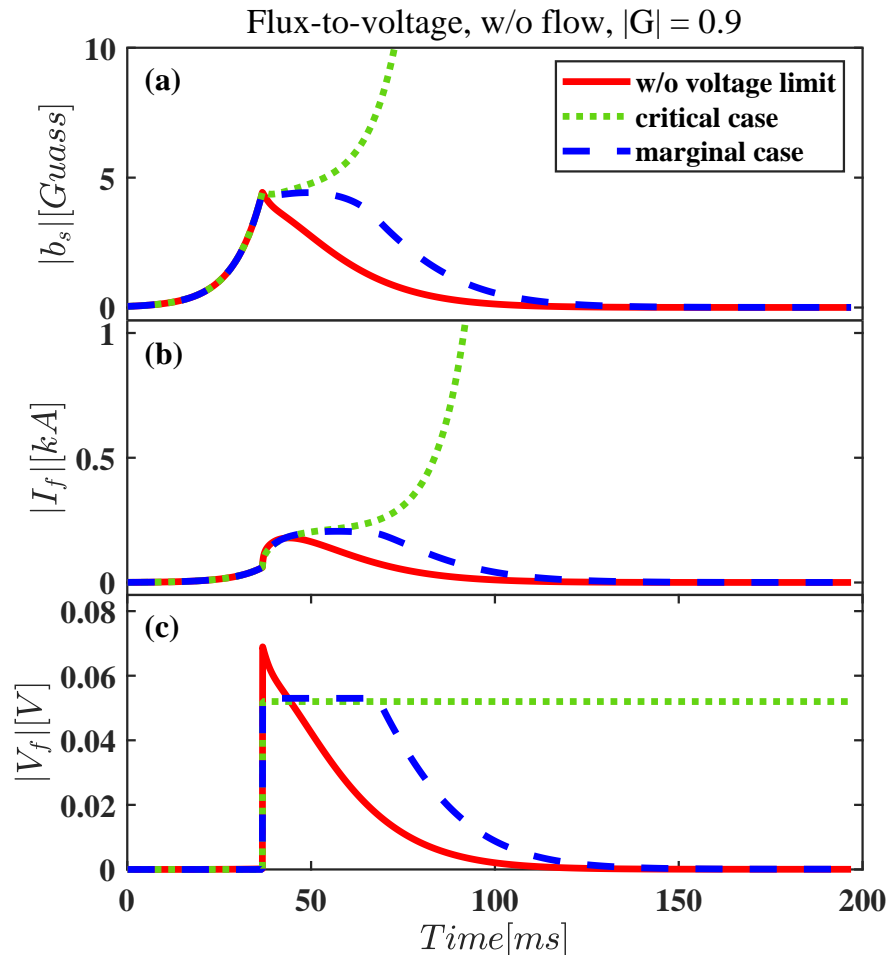


Figure 10. Comparison of three simulated time traces for the RWM with flux-to-voltage control scheme: linear feedback without control coil voltage limitation (blue solid line), feedback with voltage limit just above (yellow dashed line) and just below (red dotted line) the critical level. Plotted are the time traces of (a) the amplitude of the poloidal sensor signal, (b) the current amplitude in the active coils, and (c) the voltage of the active coil power supply. The control loop is closed at 37 ms. The proportional feedback gain is assumed as $|G| = 0.9$, the equilibrium is fixed at $C_\beta = 0.4$. No plasma flow effect is considered in these cases.

Results reported in Fig. 10 are further expanded to other HL-2M equilibria with varying pressure. Figure 12 shows the V_f^{\min} values in the 2D parameter space of both C_β and the plasma rotation Ω_0/Ω_A . The growth rate of the RWM is maximal as C_β approaches unity. The V_f^{\min} value also reaches the maximum at this limit, especially in the absence of the plasma flow stabilization.

It is interesting to note that the V_f^{\min} value is not always a monotonic function of C_β . For instance, at fixed flow speed $\Omega_0/\Omega_A = 0.02$, we find that the V_f^{\min} value at $C_\beta = 0.9$ is smaller than that at $C_\beta = 0.8$ or 0.7 . Detailed examination reveals that this is related to the fact that close-loop time traces exhibit oscillating behavior (not shown

Modeling active control of resistive wall mode with power saturation and sensor noise on HL-2M17

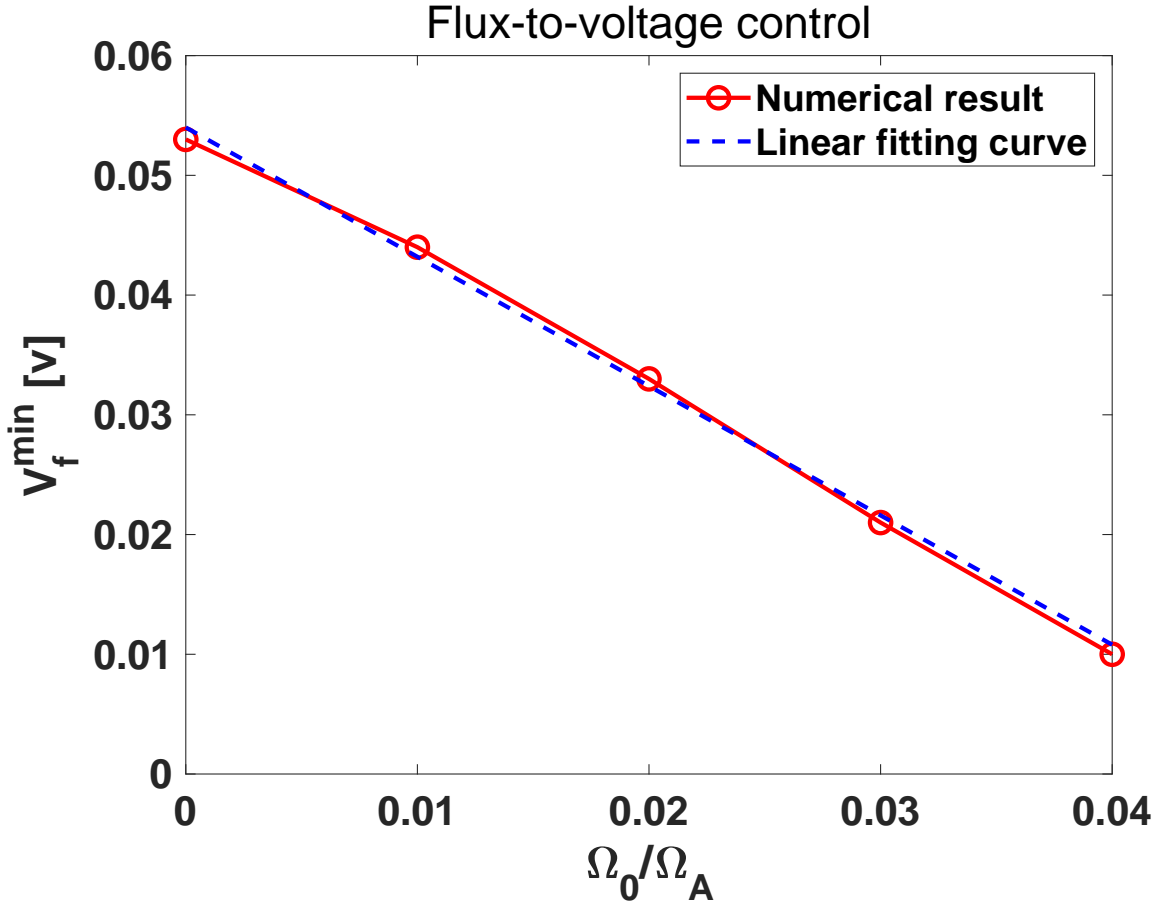


Figure 11. The required minimal voltage V_f^{\min} versus the plasma toroidal rotation frequency. The computed (solid line) and analysis fitting (dashed line) curves are plotted. The other parameters are fixed at $C_\beta = 0.4$, $\kappa_{//} = 1.5$, $|G| = 0.9$.

here) at sufficiently fast plasma flow and at $C_\beta = 0.7$ or 0.8 . On the contrary, the close-loop control voltage always monotonically decays with time at $C_\beta = 0.9$, independent of the rotation frequency.

As the final stage of study, we now also inject the Gaussian white noise into the sensor signal in the close-loop simulations. Figure 13 shows three examples of the simulated time traces for the close-loop system. All the input parameters are identical among these three cases, except the three different samples for the sensor noise (with the same standard deviation as shown in Fig. 13(d)) which are machine-generated during the simulations. The resulting close-loop performance, in the presence of the control power limitation, is however drastically different. In particular, in the case shown in green, the RWM control is eventually lost after about 150 ms simulation time. Without the control voltage limitation, the mode remains stable though the sensor noise does affect the control performance. Note that the sensor signal noise level is fixed in this study, with the standard deviation of $\sigma_{\text{noise}} = 0.1$ G following a multi-machine database analysis reported in Ref. [38].

Modeling active control of resistive wall mode with power saturation and sensor noise on HL-2M18

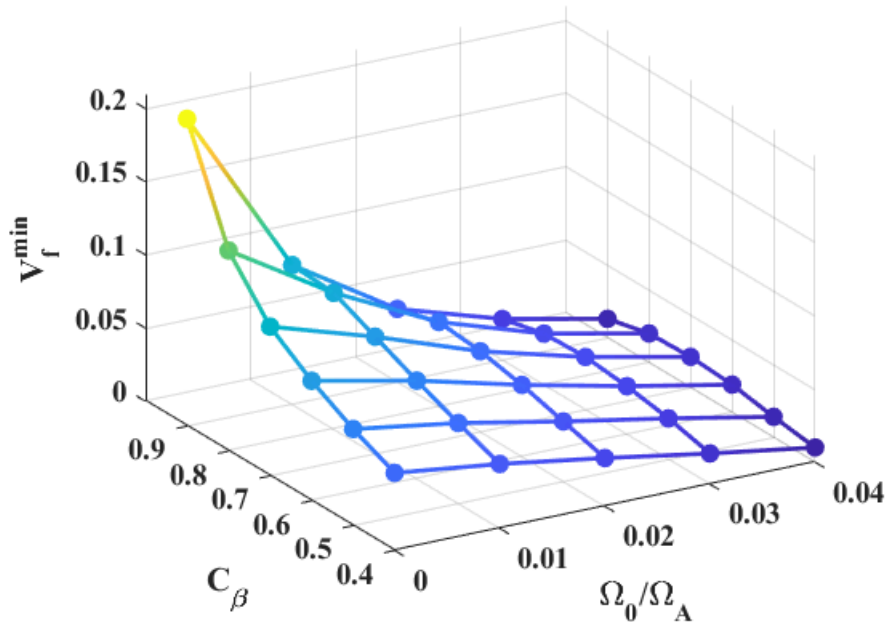


Figure 12. The MARS-F computed minimal voltage versus the normalized plasma rotation frequency. Here plasma pressure varies from $C_\beta = 0.4$ to 0.9 . The other parameters are fixed at $\kappa_{//} = 1.5$, $|G| = 0.9$.

We also note that the required voltage for controlling the RWM on HL-2M is generally small even in the presence of the sensor signal noise. The control voltage will certainly increase if we operate the AT plasma beyond the target pressure. Moreover, the busbar resistance and other resistant elements in the control circuit will further increase the overall power required for controlling the mode in real experiments. The required control coil current is about 0.6 kA according to Fig. 13(c) (again for the target plasma). The designed maximal current for the in-vessel magnetic coils is 10 kA on HL-2M. Preliminary estimate shows that ~ 5 kA current is needed to control type-I ELMs on HL-2M, utilizing the same set of in-vessel coils. This leaves a significant margin for the combined control of the ELM and the RWM on HL-2M.

Figure 13 shows the statistic nature of the feedback system when the sensor signal noise is included and the control voltage is limited. To better quantify the results, we repeat 20 times the initial value simulation for each (deterministic) parameter setup, with different noise samples that have the same standard deviation. If the close-loop remains stable for 18 (i.e. 90%) out of 20 simulations, similar to those shown by red and blue curves in Fig. 13, we define the applied voltage limitation level as acceptable, or in other words the RWM control is successful with the given voltage limit.

Our eventual goal here is to identify the minimal voltage saturation level V_f^{\min} , above which the RWM control is still successful (in the above sense) in the presence of the sensor signal noise. Figure 14 compares the simulated V_f^{\min} assuming three different plasma rotation frequencies. With each rotation, we also vary the feedback

Modeling active control of resistive wall mode with power saturation and sensor noise on HL-2M19

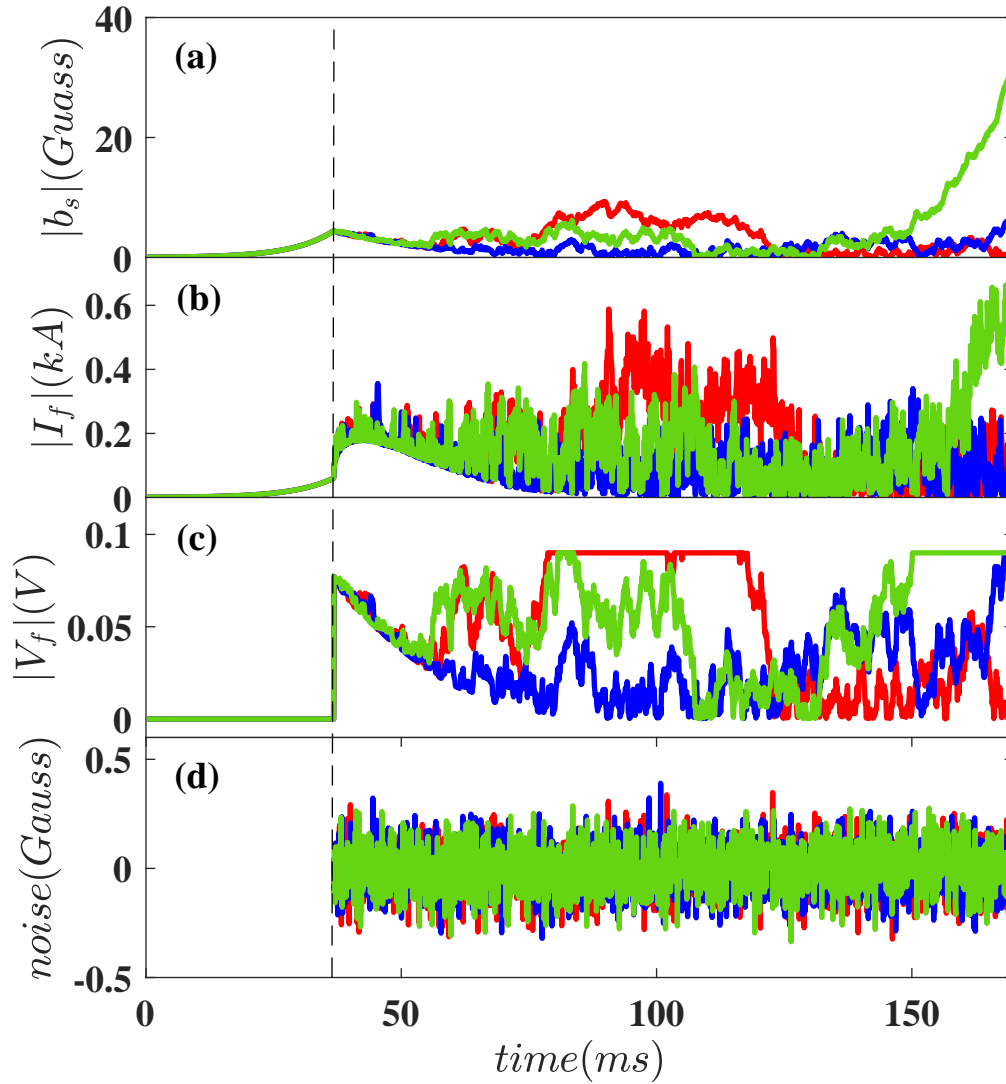


Figure 13. Three examples of initial value simulation of the $n = 1$ RWM feedback with control voltage saturation and sensor signal noise. All the input parameters are identical in these simulations, except that different samples of sensor signal noise are assumed. Plotted are (a) amplitude of the poloidal sensor signal, (b) the control coil current, (c) the control voltage, and (d) samples of the machine-generated noise with Gaussian distribution and standard deviation of $\sigma_{\text{noise}} = 0.1$ G. The feedback system closed at 37 ms. The other parameters are fixed at $C_\beta = 0.4$, $|G| = 1$, $\Omega_0 = 0$. The control voltage limit is set at $V_f^{\text{lim}} = 0.09$ V.

Modeling active control of resistive wall mode with power saturation and sensor noise on HL-2M20

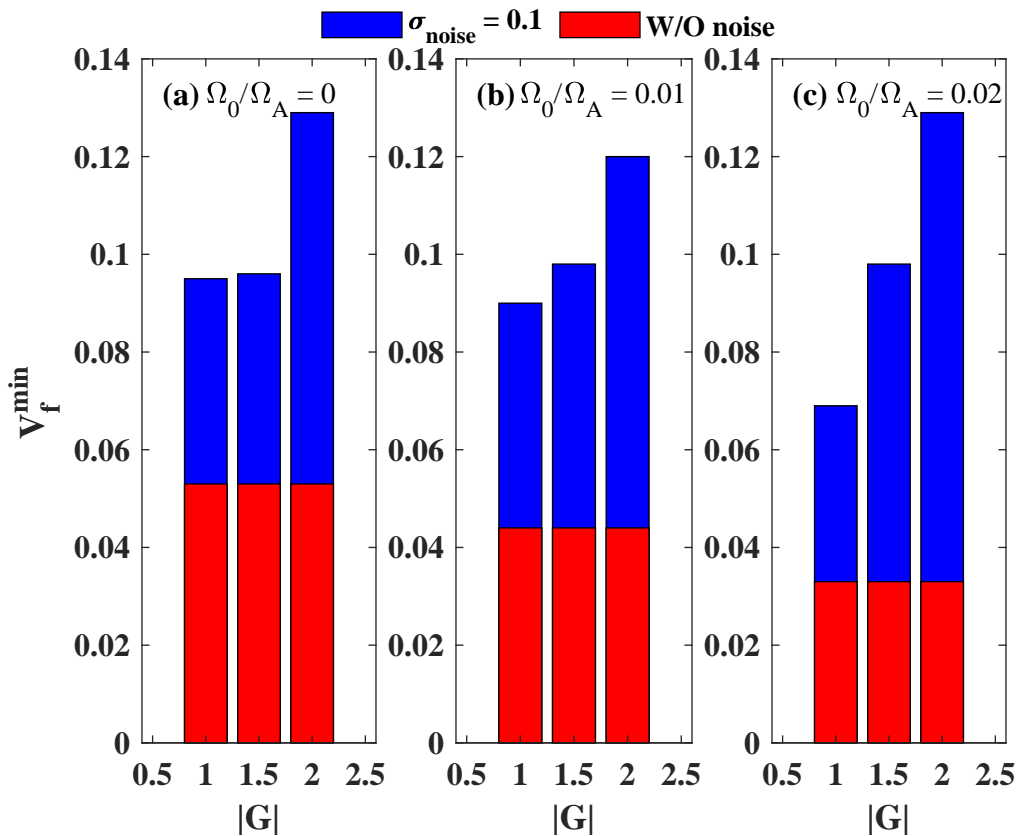


Figure 14. The minimal voltage V_f^{\min} versus feedback gain in the presence of sensor noise for different plasma rotation frequencies: (a) without flow, (b) $\Omega_0/\Omega_A = 0.01$, (c) $\Omega_0/\Omega_A = 0.02$. The minimal voltage needed to control the $n = 1$ RWM, in the absence of the sensor signal noise, is shown in red cubes. The minimal voltage in the presence of sensor noise is evaluated from 20 initial value runs for each voltage limit, and the limit with 90% success rate (to stabilize the RWM) is defined as the minimal voltage V_f^{\min} . The plasma pressure is fixed at $C_\beta = 0.4$.

gain amplitude. In the absence of the sensor signal noise (histograms in red), much smaller values of V_f^{\min} can be tolerated, where the RWM control is still successful. The V_f^{\min} value decreases with increasing plasma flow, again indicating favorable stabilization effect brought in by the plasma flow. The V_f^{\min} value however does not change with increasing feedback gain. This interesting result was also analytically demonstrated in Ref. [24].

With inclusion of the sensor signal noise (histograms in blue), we find three major changes. (i) The overall tolerable voltage limit is roughly doubled, compared to that without noise. (ii) The plasma flow still generally plays a favorable role in reducing V_f^{\min} , but this does not hold for all cases. Exceptions include the case with $|G| = 2$ and $\Omega_0/\Omega_A = 0.02$. (iii) At a given rotation, the V_f^{\min} value now depends on the feedback gain amplitude. In fact, the tolerable voltage limit generally increases with increasing feedback gain. Taking the extreme example shown in Fig. 14 (c), the V_f^{\min} value at $|G| = 2$ is about twice of that at $|G| = 1$. This value (at $|G| = 2$) in turn is about four

Modeling active control of resistive wall mode with power saturation and sensor noise on HL-2M21

times larger than that without the sensor signal noise. This shows that for the RWM control on HL-2M, the sensor signal noise is indeed a sensitive issue, that need to be carefully taken into account when designing the RWM control system.

4. Conclusion and discussion

This work studies the $n = 1$ RWM control with plasma flow, magnetic feedback, and a combination of both on the HL-2M tokamak. As for the target plasma, we consider a high performance equilibrium with $I_p = 2$ MA, $B_0 = 2.2$ T and $\beta_N = 4.31$ ($C_\beta = 0.4$) designed for the AT scenario on HL-2M. Our primary goal is to take into account realistic control elements, i.e. the control power saturation and sensor signal noise issue, while quantifying various control parameters for the RWM.

Within the fluid model, which represents a conservative estimate for the RWM stability, we find that the subsonic plasma toroidal flow passively stabilizes the RWM only in a narrow region in the 2D parameter space $C_\beta - \Omega_0/\Omega_A$. The critical on-axis rotation frequency, for marginal stability of the RWM without feedback, is quantified via a linear fitting curve of $\Omega_0/\Omega_A = 0.152 C_\beta$, as the plasma pressure varies.

Magnetic feedback can fully stabilize the RWM on HL-2M. Without considering the voltage limitation and the sensor signal noise, we find that plasma flow helps active control of the mode, by reducing the required critical feedback gain. This synergistic effect can be quantified by analytic fitting formulae $|G_{\text{cri}}| = -38.6 (\Omega_0/\Omega_A)^2 - 9.6 \Omega_0/\Omega_A + 0.66$ for the flux-to-current control scheme, and $|G_{\text{cri}}| = -47.9 (\Omega_0/\Omega_A)^2 - 11.5 \Omega_0/\Omega_A + 0.66$ for the flux-to-voltage control, based on the MARS-F computed eigenvalue results. These fitting formulae also confirm the analytic observation from Eq. (6), that the critical feedback gain is the same between the two control schemes at vanishing plasma flow.

MARS-F initial value simulations have also been carried out for the RWM feedback on HL-2M. In the absence of the sensor signal noise, the lowest control voltage saturation level, below which the RWM control is lost, is found to roughly satisfy a linear relation to the plasma flow frequency $V_f^{\text{min}} = -1.08 \Omega_0/\Omega_A + 0.054$ for the HL-2M target equilibrium, indicating that subsonic plasma flow is effective in relaxing the control power requirement for the RWM feedback stabilization.

The presence of the sensor signal noise substantially modifies the feedback results. Via statistical treatment, we find that the sensor signal noise, with the standard deviation of 0.1 G on HL-2M, roughly doubles the required control voltage (for successful mode control). The synergistic stabilization effect due to the plasma flow is somewhat weakened by the presence of the sensor signal noise. At a given rotation, the tolerable voltage limit generally increases with increasing feedback gain. At the toroidal rotation of $\Omega_0/\Omega_A = 0.02$, we find that the tolerable voltage limit at $|G| = 2$ is about twice of that at $|G| = 1$. This value (at $|G| = 2$) in turn is about four times larger than that without the sensor signal noise.

This work does not consider the derivative control action or other more advanced

Modeling active control of resistive wall mode with power saturation and sensor noise on HL-2M22

controller design. This remains a future study. The derivative action is not good when there is sensor noise, since taking time derivative will significantly amplify the sensor signal noise [26]. As a result, this may drastically increase the voltage and current needed in the active coils to control the RWM.

This work also neglected the drift kinetic stabilization effect on the RWM, due to thermal and/or energetic particles. This leads to conservative estimate of the passive stability of the mode on HL-2M. Thermal particle drift kinetic stabilization has been found to stabilize the RWM on HL-2M at slow toroidal flow ($\Omega_0 \leq 0.006\Omega_A$) [32]. The energetic particle effect, as well as the combined effect of both passive and active control in the presence of drift kinetic stabilization, will likely yield more optimistic results on the RWM stability on HL-2M, than what we have found here. Quantitative investigation remains a future work.

Acknowledgements

This work is supported by the National Natural Science Foundation of China (NSFC) under Grant No.11805054. The work is also supported by the U.S. Department of Energy Office of Science under contracts DE-FG02-95ER54309 and DE-FC02-04ER54698. This work has been carried out within the framework of the EUROfusion Consortium and has received funding from the Euratom research and training programme 2014-2018 and 2019-2020 under Grant Agreement No. 633053. The views and opinions expressed herein do not necessarily reflect those of the European Commission.

References

- [1] T.C. Hender *et al* 2007 *Nucl. Fusion* **47** S128
- [2] Troyon F *et al* 1984 *Plasma Phys. Control. Fusion* **26** 209–15
- [3] A. Bondeson and D. Ward 1994 *Phys. Rev. Lett.* **72** 2709
- [4] M. S. Chu *et al* 1995 *Phys. Plasmas* **2** 2236
- [5] B. Hu and R. Betti 2004 *Phys. Rev. Lett.* **93** 105002
- [6] S. Sabbagh *et al* 2006 *Nucl. Fusion* **46** 635
- [7] H. Reimerdes *et al* 2007 *Phys. Rev. Lett.* **98** 055001
- [8] M. Takechi *et al* 2007 *Phys. Rev. Lett.* **98** 055002
- [9] Y. Q. Liu *et al* 2008 *Phys. Plasmas* **15** 112503
- [10] J. W. Berkery *et al* 2010 *Phys. Plasmas* **17** 082504
- [11] G. Z. Hao *et al* 2012 *Phys. Plasmas* **19** 032507
- [12] Y. He *et al* 2014 *Phys. Rev. Lett.* **113** 175001
- [13] C. Liu *et al* 2015 *Nucl. Fusion* **55** 063022
- [14] Y. Q. Liu and A. Bondeson 2000 *Phys. Rev. Lett.* **84** 907
- [15] Y. Q. Liu *et al* 2000 *Phys. Plasmas* **7** 3681
- [16] C. M. Fransson *et al* 2000 *Phys. Plasmas* **7** 4143
- [17] M. Okabayashi *et al* 2001 *Phys. Plasmas* **8** 2071
- [18] E. D. Fredrickson *et al* 2001 *Plasma Phys. Control. Fusion* **43** 313
- [19] A. Garfalo *et al* 2001 *Nucl. Fusion* **41** 1171
- [20] A. K. Sen *et al* 2003 *Phys. Plasmas* **10** 4350
- [21] E. J. Strait *et al* 2004 *Phys. Plasmas* **11** 2505

1
2
3 *Modeling active control of resistive wall mode with power saturation and sensor noise on HL-2M23*

- 4
5 [22] M. Okabayashi *et al* 2009 *Nucl. Fusion* **49** 125003
6 [23] Z. Wang *et al* 2011 *Nucl. Fusion* **51** 053004
7 [24] L. Li *et al* 2012 *Phys. Plasmas* **19** 012502
8 [25] S. Wang *et al* 2018 *Fusion Sci. Technol.* **73** 519
9 [26] S. Wang *et al* 2019 *Nucl. Fusion* **59** 096021
10 [27] Q. Li *et al* 2015 *Fusion Eng. Des.* **96-97** 338-342
11 [28] B. Li *et al* 2019 *Fusion Eng. Des.* **147** 111229
12 [29] L. Xue *et al* 2017 *Nucl. Fusion* **57** 056029
13 [30] G. L. Xia *et al* 2014 *Plasma Phys. Control. Fusion* **56** 095009
14 [31] G. L. Xia *et al* 2015 *Nucl. Fusion* **55** 093007
15 [32] G. L. Xia *et al* 2019 *Nucl. Fusion* **59** 016017
16 [33] A. Bondeson and M. S. Chu 1996 *Phys. Plasmas* **3** 3013
17 [34] Y. Q. Liu *et al* 2004 *Nucl. Fusion* **44** 232-242
18 [35] R.J. La Haye *et al* 2004 *Nucl. Fusion* **44** 1197
19 [36] A. Bondeson *et al* 2002 *Nucl. Fusion* **42** 768
20 [37] Y. Q. Liu 2007 *Computer Physics Communications* **176** 161-169
21 [38] Y. Q. Liu *et al* 2017 *Fusion Sci. Technol.* **70** 387
22
23
24
25
26
27
28
29
30
31
32
33
34
35
36
37
38
39
40
41
42
43
44
45
46
47
48
49
50
51
52
53
54
55
56
57
58
59
60